Gel phase in hydrated calcium dipicolinate

Pankaj Rajak, Ankit Mishra, Chunyang Sheng, Subodh Tiwari, Aravind Krishnamoorthy, Rajiv K. Kalia, Aiichiro Nakano, and Priya Vashishta

Citation: Appl. Phys. Lett. **111**, 213701 (2017);
View online: https://doi.org/10.1063/1.5000394
View Table of Contents: http://aip.scitation.org/toc/apl/111/21
Published by the American Institute of Physics

Gel phase in hydrated calcium dipicolinate

Pankaj Rajak, Ankit Mishra, Chunyang Sheng, Subodh Tiwari, Aravind Krishnamoorthy, Rajiv K. Kalia, Aiichiro Nakano, and Priya Vashishta
Collaboratory for Advanced Computing and Simulations, Department of Physics and Astronomy, Department of Computer Science, Department of Chemical Engineering and Materials Science, Department of Biological Sciences, University of Southern California, Los Angeles, California 90089-0242, USA

(Received 15 August 2017; accepted 11 October 2017; published online 20 November 2017)

The mineralization of dipicolinic acid (DPA) molecules in bacterial spore cores with Ca^{2+} ions to form Ca-DPA is critical to the wet-heat resistance of spores. This resistance to "wet-heat" also depends on the physical properties of water and DPA in the hydrated Ca-DPA-rich protoplasm. Using reactive molecular dynamics simulations, we have determined the phase diagram of hydrated Ca-DPA as a function of temperature and water concentration, which shows the existence of a gel phase along with distinct solid-gel and gel-liquid phase transitions. Simulations reveal monotonically decreasing solid-gel-liquid transition temperatures with increasing hydration, which explains the experimental trend of wet-heat resistance of bacterial spores. Our observation of different phases of water also reconciles previous conflicting experimental findings on the state of water in bacterial spores. Further comparison with an unmineralized hydrated DPA system allows us to quantify the importance of Ca mineralization in decreasing diffusivity and increasing the heat resistance of the spore. https://doi.org/10.1063/1.5000394

Bacterial spores are resistant to extreme temperatures and pressures and environments of low nutrient availability.[1–4] Under such adverse conditions, vegetative cells undergo the process of sporulation, resulting in the formation of dormant spores.[2,5–7] These spores have a wide range of lifespans ranging from a couple of days to millions of years.[8] The physical and chemical resistance of these spores, their ability to germinate after sub-lethal damage, and their suitability for genetic manipulations are of great practical and commercial importance.[9]

Bacterial spores have a complex, layered structure, comprising a large and loose-fitting outermost exosporium, followed by an inner spore coat containing over 50 proteins.[2,10] Further inward lies the outer membrane, which has no major contribution to spore's resistance to heat or permeability.[11] The outer membrane is followed by the cortex which is made up of peptidoglycan (PG), which is responsible for the decrease in the water content inside the core. The inner most part of the spore is the spore core, and it consists of metabolic enzymes, proteins, DNA, and Dipicolinic Acid (DPA), and its mineralized forms contain divalent cations such as Ca^{2+}, Mg^{2+}, and Mn^{2+}.[11]

Various techniques, including heat, chemical, and radioactive treatments, have been proposed for the sterilization of harmful bacterial spores in the defense and food industries. Recently, nitrogen cold atmospheric plasma has been used as a biocide because it causes changes in surface morphology and loss of spore integrity.[12] High pressure treatment of spores has been applied, resulting in their loss of viability. This is primarily attributed to the loss of DPA or due to the possible oxidative losses in the absence of DPA.[13] Chemical treatments involving decontaminating agents like dimethyldioxirane (DMDO) have also been studied and found to initiate possible oxidative losses due to a variety of oxidation reactions.[14] However, these sterilization techniques carry disadvantages such as increased energy consumption and treatment under extreme conditions associated with plasma production. Considering these factors, wet-heat treatments are considered a better alternative for killing spores.[15,16] Application of wet-heat in the range of 80–95 °C leads to the loss of viability in the spore core, resulting in compromised germination and no outgrowth leading to spore death. Furthermore, it has been observed that heat resistance of bacterial spore decreases with the increasing hydration content during wet-heat treatment.[17]

Although the role of DPA in its mineralized form (chelated with Ca^{2+} to form Ca-DPA) in affecting the wet-heat resistance has been quantified,[16,18–22] the mechanism responsible for this improved heat resistance is not well understood. A leading hypothesis posits that the heat resistance is an outcome of the suppressed enzyme activity and protein agglomeration due to the extremely low diffusivity in the Ca-DPA rich spore core.[23] Further, the structure of water molecules in this material system also remains unresolved, with prior experiments suggesting both mobile liquid-like and immobile glassy configurations of water molecules in the spore core. Recent nuclear magnetic resonance experiments indicate that water is immobilized in the spore cores of *Bacillus subtilis* and *Bacillus pumilus*, i.e., the spore core is glass-like with no significant diffusivity of water molecules,[24] rather than being gel-like.[15,16] On the contrary, measurements of water ^{2}H and ^{17}O spin relaxation rates in D_2O-exchanged *Bacillus subtilis* indicate high water mobility, indicating a gel-like configuration of water molecules.[23] Here, we reconcile these findings using reactive molecular dynamics (RMD) simulations to quantify the structure and diffusivity of water molecules[25,26] as a function of temperature and water content. Our simulation results clearly distinguish

between solid, gel-like, and molten states in the temperature-water content phase diagram. Understanding molecular mobility and phase transformations in the spore core may help explain the role of the Ca-DPA rich core matrix in arresting protein conformational changes, agglomeration, and denaturation and may shed light on the wet-heat resistance of bacterial spores.

We use RMD simulations based on first principles-derived reactive force fields (ReaxFF)[27–30] to calculate the mean square displacement (MSD) and coefficient of self-diffusion of water and DPA molecules in hydrated Ca-DPA simulation cells as a function of temperature and level of hydration. We have developed a force field for Ca-DPA·3H_2O that reproduces experimental lattice constants and important bond-lengths for this system. Our main motivation to use the reactive force field was for hydrated systems. Figure 1 shows the unit cell of the Ca-DPA crystal containing four Ca ions and four DPA molecules along with twelve water molecules that are bound to Ca ions. In addition, the figure also contains 11 water molecules that represent excess added water found in Ca-DPA systems at higher hydration levels. The crystal structure of the native form of calcium dipicolinate [Ca-DPA·3H_2O][22] contains two types of H_2O molecules, distinguishable by the number of calcium ions in their coordination shell. We refer to H_2O molecules containing one and two calcium ions in their coordination shells as H_2O^1 and H_2O^2, respectively. Wet-heat treatments lead to increased hydration of the Ca-DPA matrix, leading to a composition of [Ca-DPA·3H_2O]$_4$ + nH_2O—containing n added water molecules per unit cell, denoted as H_2O^0, that are not bonded to any of the Ca ions in the Ca-DPA crystal. These nominally unbound water molecules occupy interstices within the hydrated CA-DPA structure. For the rest of this paper, we refer to the oxygen atoms found in H_2O^1, H_2O^2, and H_2O^0 as O^1, O^2, and O^0, respectively, and the oxygen in the DPA molecule as O^{DPA}. We will use their RMD trajectories to monitor the mean square displacement (MSD) and determine the coefficient of self-diffusion of the three types of H_2O and DPA molecules.

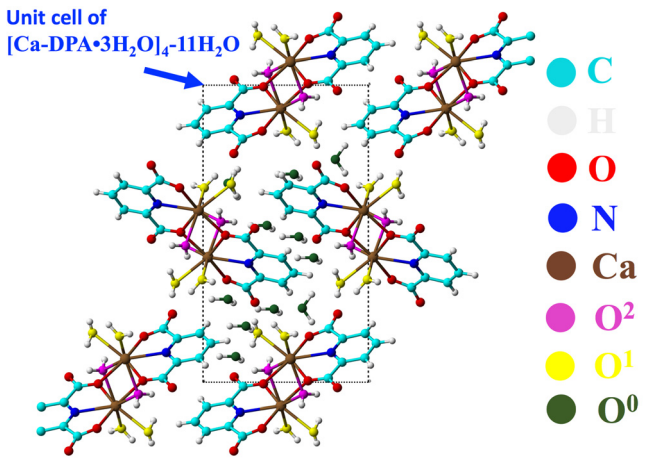

FIG. 1. Configuration of [Ca-DPA·3H_2O]$_4$ + 11H_2O (water content of 33.5 wt. % H_2O), prepared from [Ca-DPA·3H_2O]$_4$ by adding 11 additional water molecules to the unit cell (outlined in black). O^1 (in yellow) and O^2 (in magenta) are O atoms of singly and doubly coordinated water molecules with calcium of Ca-DPA, respectively, and O^0 (in green) is the oxygen atom of the added water molecules.

The calculated MSD values are also used to distinguish between different material phases since the MSD for a system in a solid state is constant in time for large times, while a linear dependence of MSD with time indicates a fluid phase. In RMD simulations, the time evolution of atomic trajectories is determined by an environment-dependent force field based on the concept of bond order. The ReaxFF describes chemical bond breakage and formation by introducing bond orders and charge transfer between atoms based on a charge-equilibration approach. We use an in-house scalable parallel reactive molecular dynamics (RMD) code, in which the time-consuming iterative determination of atomic charges is replaced by a computationally efficient extended Lagrangian scheme.[31]

We start our RMD simulations with equilibrated zero-pressure simulation cells of the hydrated Ca-DPA crystal, where the water concentration ranges between 20.8 and 33.54 wt. %. Zero-pressure configurations are obtained for all hydrated Ca-DPA systems at various temperatures using the following procedure. The initial structures of Ca-DPA are first relaxed by setting atomic velocities to zero at every 100 steps for a total of 20,000 steps, where the unit time step is 0.3 fs. Subsequently, the systems are heated to −173 °C and thermalized for 200,000 time steps in canonical (NVT) ensemble. These relaxed configurations are then expanded in steps of 1.5% by volume, and each of these expanded systems is heated up to 400 °C in steps of 50 °C. The length of each of these runs is again 200,000 steps. After that, the zero-pressure configuration for each of these expanded systems is obtained from their pressure-temperature plot. These zero-pressure systems are further relaxed for 1000 ps for the MSD calculation. It can be observed that the volume of the Ca-DPA simulation cell expands linearly with the water content, increasing by 33.5% as the water content increases from 20.8 wt. %, [Ca-DPA·3H_2O]$_4$ to 33.54 wt. %, [Ca-DPA·3H_2O]$_4$ + 11H_2O [Fig. 2(a)].

Figure 2(b) shows representative MSD of the three types of water molecules in a molten Ca-DPA system, [Ca-DPA·3H_2O]$_4$ + 11H_2O. Another important observation in the MSD results is that the doubly Ca-coordinated H_2O^2 molecule diffuses more slowly than the singly bound H_2O^1 molecule. These results suggest an important role of Ca^{2+} ions in controlling the dynamics of water molecules in the spore core, which will be discussed more detail below.

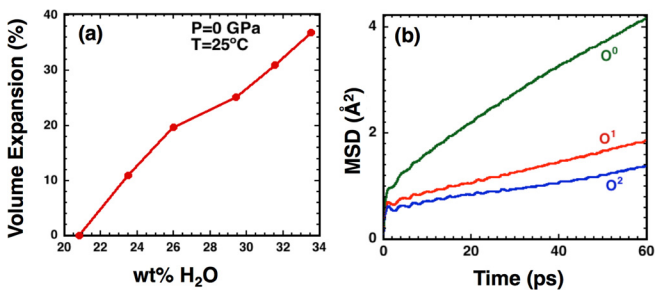

FIG. 2. (a) Volume expansion (%, relative to the volume of [Ca-DPA·3H_2O]$_4$) required to obtain the zero pressure configuration in the [Ca-DPA·3H_2O]$_4$ + nH_2O crystal as a function of water content at 25 °C. (b) Mean-square displacement of three different types of water molecules present in a representative molten system, [Ca-DPA·3H_2O]$_4$ + 11H_2O (will become 1 ns above 100 C).

The length of our MD simulations is 1000 ps. The length of the correlation function $\langle R(t)^2 \rangle$ is 60 ps; however, 600 initial conditions are used for better averages (Fig. 3). Self-diffusion coefficients, D, for the various molecules are computed from the derivative of the MSD with time t using the following equation:

$$D = \frac{1}{6} \times \left\langle \frac{d\,MSD(t)}{d\,t} \right\rangle. \quad (1)$$

Figure 3 shows computed diffusivities for different types of H_2O molecules and DPA for temperatures ranging from 25 °C to 320 °C at different levels of hydration. Comparison of Figs. 3(b)–3(d) shows that the threshold temperature for the onset of diffusion is the lowest for the mobile O^0 species followed by O^1 and O^2 species consistent with the relative degree of binding to the Ca-DPA matrix. In contrast to the relatively mobile water molecules, computed diffusivities of DPA molecules are approximately one order of magnitude lower [Fig. 5(a)], reflecting their greater size, weight, and higher melting point.

This quantification of constant of self-diffusion can be used to distinguish between liquid-like, gel-like, and crystal-like behavior of water and DPA molecules in the spore. In our analysis, we consider Ca-DPA and water diffusivities greater than 3×10^{-8} cm^2/s and 1.2×10^{-7} cm^2/s to represent the onset of liquid-like mobility, based on the magnitude to measure the diffusivity of confined water molecules in silica gels.[32]

To better understand the physical state of the water in hydrated Ca-DPA, we monitor the trajectories of different types of water molecules in Ca-DPA at 25 °C and above 100 °C. The trajectories of water molecules in Figs. 4(a) and 4(b) and corresponding movies in the Multimedia views show that water molecules are confined to interstices in the Ca-DPA·11H_2O (32%) matrix at 25 °C but show more extended long-range diffusion at 400 °C.

This diffusivity-based characterization into liquid and solid phases as a function of temperature and water content is summarized in a phase diagram of the spore core [Fig. 5(a)]. It is noticeable that low hydration and low temperatures lead to a configuration of largely immobile Ca-DPA and water molecules representing the solid phase. This corresponds to the experimentally observed solid phase of the spore core that is hypothesized to be responsible for greater heat resistance by suppression of diffusivity and conformational freedom required for denaturation. Over a narrow

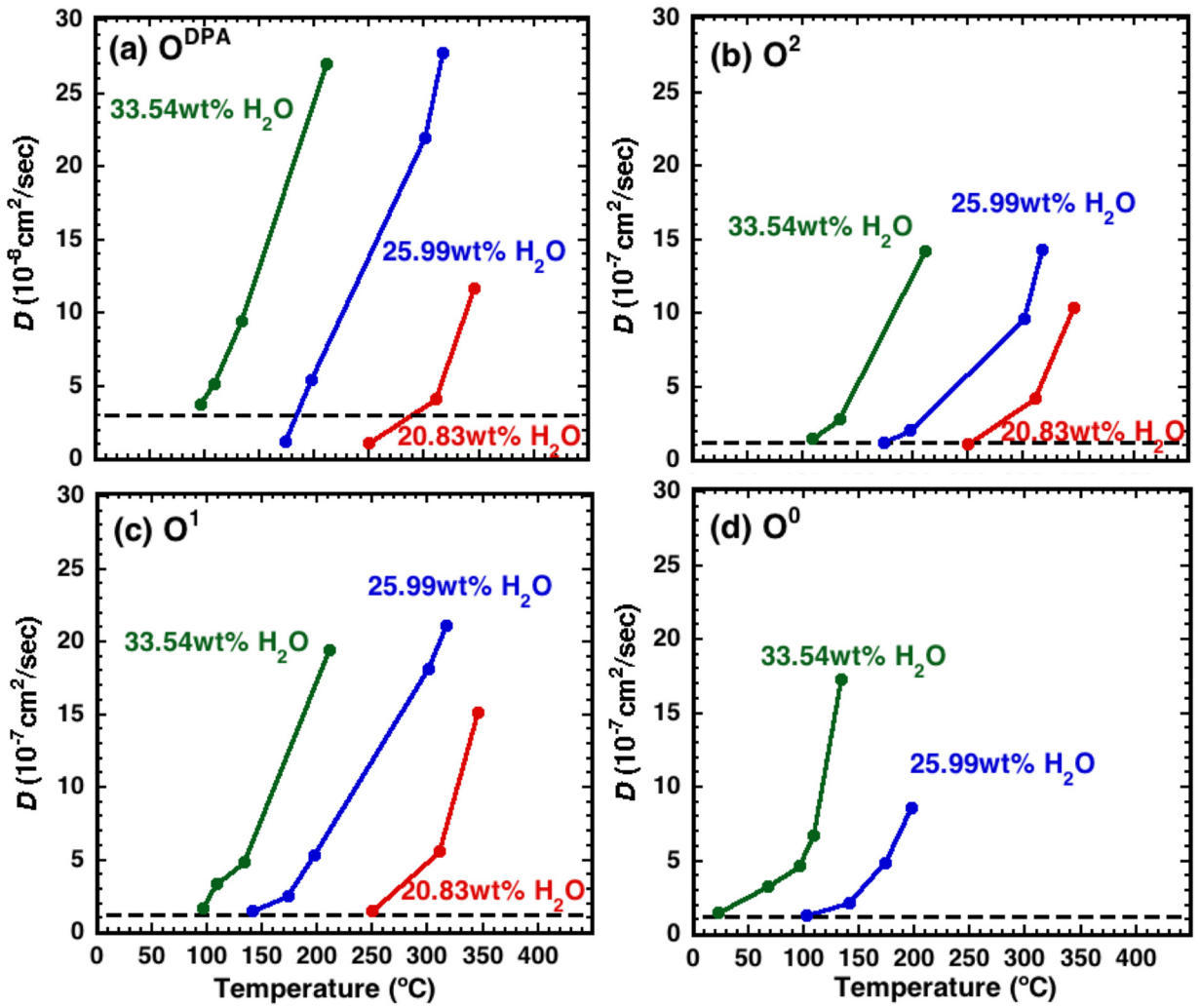

FIG. 3. Diffusion constant with the increasing value for (a) O^{DPA}, (b) O^2, (c) O^1, and (d) O^0 present in the [Ca-DPA·3H_2O]$_4$ + nH_2O system. Dotted lines denote the value above which the system is considered to be liquid. The diffusion threshold for DPA and water is 3×10^{-8} and 1.2×10^{-7} cm^2/s, respectively.

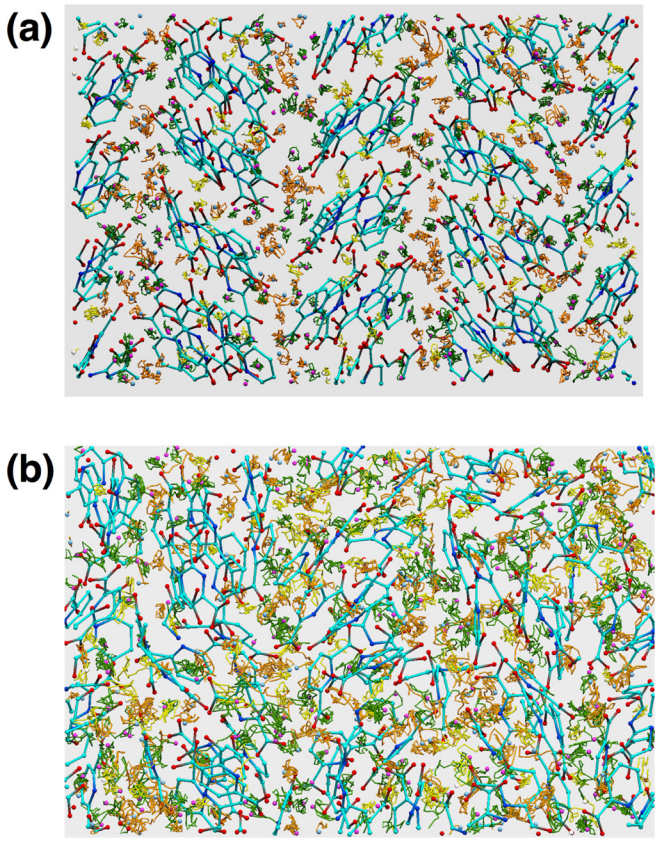

FIG. 4. Snapshots of RMD simulations at (a) 25 °C and (b) 400 °C. Trace of the trajectory of each type of water molecules in Ca-DPA for 2.4 ps is drawn as a line. Light yellow lines denote the O^1 atoms, green lines denote the O^2 atoms, and dark yellow lines denote the O^0 atoms. Multimedia view: https://doi.org/10.1063/1.5000394.1; https://doi.org/10.1063/1.5000394.2

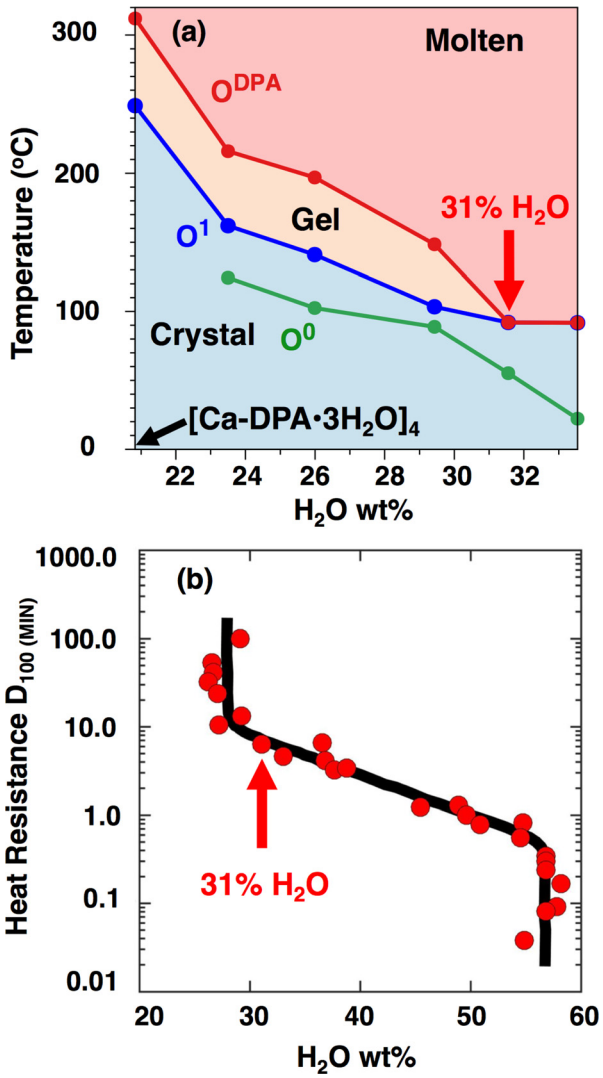

FIG. 5. (a) Melting points (i.e., temperature for the onset of long-range diffusion) of DPA (red), O^1 (blue), and O^0 (green) as a function of the water content in Ca-DPA crystal. The red region indicates the molten state of [Ca-DPA·3H_2O] + nH_2O, and the blue region indicates the crystalline region. The intermediate orange region denotes the gel phase, where water molecules are mobile, and DPA molecules are immobile and the red molten phase is composed of molten DPA and H_2O molecules. (b) Experimental estimation of wet-heat resistance dependence on the water content of protoplast. Replotted with data from Ref. 17.

range of intermediate temperatures (250 °C to 310 °C), Ca-DPA molecules in the [Ca-DPA·3H_2O] crystal remain immobile but their hydration shells show significant long-range diffusion and liquid-like behavior. The diffusion of added water (n = 2 to 11 in [Ca-DPA·3H_2O]$_4$ + nH_2O) in the temperature range of 250 °C to 92 °C leads to a spore core more amenable to processes that precede spore death. We refer to this phase as the "gel" phase, denoted by light orange color in Fig. 5. A further increase in the level of hydration leads to liquid-like diffusion in both the Ca-DPA and water bound with Ca^{2+} ions and gives rise to a fully molten phase.

Most importantly for the moist-heat treatment of bacterial spores, we demonstrate that the temperature required for the solid-gel and gel-molten phase transformations decreases with increasing hydration and saturates at 92 °C for the water content beyond 31 wt. % H_2O. This observation is consistent with experimental measurements of heat resistance of spore cores in contact with wet-heat [Fig. 5(b)], which shows that the heat resistance of the spore core starts decreasing when the water content in the protoplast becomes more than 30%.[17]

The phase diagram in Fig. 5 is dominated by phase transitions involving Ca-coordinated water molecules, H_2O^1 and H_2O^2. In order to understand the effect of Ca mineralization on the phase transformations, we compare Fig. 5 to the phase diagram of the Ca-free hydrated DPA crystal (Fig. 6) at different temperatures and different water contents, specifically 0 wt. % (anhydrous DPA),[33] 9.7 wt. % (DPA monohydrate, DPA·H_2O),[34] and 17.7 wt. % (DPA dihydrate, DPA·2H_2O).

Similar to the hydrated Ca-DPA phase diagram in Fig. 5, the transition temperatures for the solid-gel and gel-liquid phase transitions decrease with increasing hydration from pure anhydrous DPA to DPA monohydrate to DPA dihydrate. Figure 5 shows the temperature for the onset of long-range diffusion of DPA and water molecules dropping from 400 °C in anhydrous DPA to 260 °C in DPA·H_2O (9.7 wt. % H_2O) and subsequently to 180 °C in DPA·2H_2O (17.7 wt. % H_2O). For a more direct illustration of the impact of Ca mineralization on the heat resistance, we compare the melting point (i.e., gel-molten phase transition temperature) of DPA·2H_2O with 18 wt. % H_2O (180 °C) to that of [Ca-DPA·3H_2O]$_4$ with 21 wt. % H_2O (310 °C). It is notable that the Ca-mineralized [Ca-DPA·3H_2O] has a significantly higher melting point even though it has a higher water content.

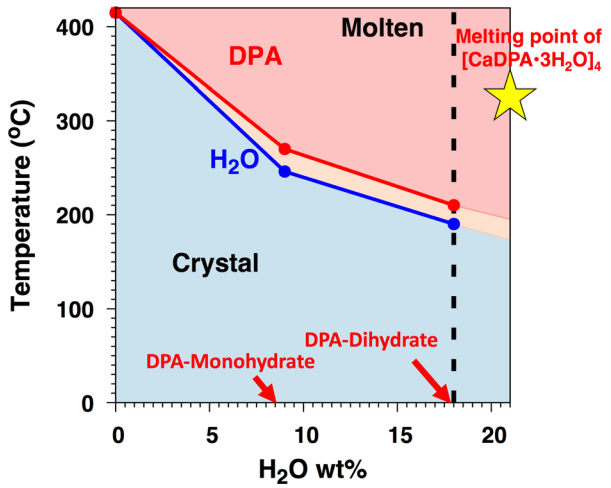

FIG. 6. Melting point of un-mineralized DPA (red) and water as a function of the water content in DPA·nH_2O. The red region indicates the molten state of the DPA·nH_2O system, and the blue region indicates the crystalline phase. The intermediate orange region denotes the gel phase, where water molecules are mobile, and DPA molecules are immobile. The phase diagram is extrapolated 18 wt. % (dashed black line) to show comparison with the hydrated Ca-DPA system with a water concentration of 21 wt. %.

In conclusion, we used RMD simulations to identify the structure and calculate the diffusivity of water, DPA, and Ca-DPA molecules as a function of temperature and hydration. The analysis described here has three main conclusions. First, it helps to reconcile outstanding differences in experimental characterization of water molecules in bacterial spore cores. Second, we show a direct relationship between molecular diffusivities in the spore core and its extent of hydration, which helps to explain the greater heat resistance of dry bacterial spores. Further, we also calculate the impact of Ca mineralization on heat resistance of spores by quantifying the melting points of unmineralized and Ca-mineralized hydrated DPA.

This research was supported by the Defense Threat Reduction Agency Grant No. HDTRA1-14-1-0074. We thank Dr. Douglas Allen Dalton and Dr. Suhithi Peiris for their encouragement and continued support throughout this investigation. The computations were performed at the Center for High Performance Computing of the University of Southern California.

[1]R. Kort, A. C. O'Brien, I. H. M. Stokkum, S. J. C. M. Oomes, W. Crielaard, K. J. Hellingwerf, and S. Brul, Appl. Environ. Microbiol. **71**, 3556 (2005).
[2]P. Setlow, J. Appl. Microbiol. **101**, 514 (2005).
[3]Y. Li, K. Jin, S. Ghosh, P. Devarakonda, K. Carlson, A. Davis, K.-A. V. Stewart, E. Cammett, P. P. Rossi, B. Setlow, M. Lu, P. Setlow, and B. Hao, J. Mol. Biol. **426**, 1995 (2014).
[4]A. Perez-Valdespino, S. Ghosh, E. P. Cammett, L. Kong, Y. Q. Li, and P. Setlow, J. Appl. Microbiol. **114**, 1109 (2013).
[5]D. W. Hilbert and P. J. Piggot, Microbiol. Mol. Biol. Rev. **68**, 234 (2004).
[6]P. Stragier and R. Losick, Annu. Rev. Genet. **30**, 297 (1996).
[7]B. Setlow, C. A. Loshon, P. C. Genest, A. E. Cowan, and P. Setlow, J. Appl. Microbiol. **92**, 362 (2002).
[8]H. W. Vreeland and J. R. Matches, Nature **407**, 897 (2000).
[9]S. R. B. R. Sella, L. P. S. Vandenberghe, and C. R. Soccol, Microbiol. Res. **169**, 931 (2014).
[10]A. Driks, Trends Microbiol. **10**, 251 (2002).
[11]P. Setlow, Am. Soc. Microbiol. **2**, 319 (2000).
[12]H. V. B. Veen, H. Xie, E. Esveld, T. Abee, H. Matswijk, and M. N. Groot, Food Microbiol. **45**, 26 (2015).
[13]C. J. Doona, F. E. Feeherry, B. Setlow, W. Shiwei, L. William, F. C. Nichols, P. K. Talukdar, M. R. Sarker, Y. Q. Li, S. Aimee, and P. Setlow, Appl. Environ. Microbiol. **82**, 5287 (2016).
[14]M. Paul, S. Atluri, B. Setlow, and P. Setlow, J. Appl. Microbiol. **101**, 1161 (2006).
[15]S. Kaieda, B. Setlow, P. Setlow, and B. Halle, Biophys. J. **105**, 2016 (2013).
[16]B. Setlow, S. Atluri, R. Kitchel, K. K. Dube, and P. Setlow, J. Bacteriol. **188**, 3740 (2006).
[17]T. C. Beaman and P. Gerhardt, Appl. Environ. Microbiol. **52**, 1242 (1986).
[18]A. J. Salle, *Fundamental Principles of Bacteriology* (McGraw-Hill, New York, 1973), Vol. 7.
[19]J. F. Powell, Biochem. J. **54**, 210 (1953).
[20]P. Setlow and E. A. Johnson, Food Microbiol. **3**, 35 (2001).
[21]A. C. Granger, E. K. Gaidamakova, V. Y. Matrosova, M. J. Daly, and P. Setlow, Appl. Environ. Microbiol. **77**, 32 (2011).
[22]G. Strahs and R. E. Dickerson, Acta Crystallogr. B **24**, 571 (1968).
[23]E. P. Sunde, P. Setlow, L. Hederstedt, and B. Halle, Proc. Natl. Acad. Sci. U. S. A. **106**, 19334 (2009).
[24]R. G. K. Leuschner and P. J. Lillford, Microbiology **146**, 49 (2000).
[25]T. Wei, T. Huang, B. Qiao, M. Zhang, H. Ma, and L. Zhang, J. Phys. Chem. B **118**, 13202 (2014).
[26]M. C. Ho, Z. A. Levine, and P. T. Vernier, J. Membr. Biol. **246**, 793 (2013).
[27]A. C. T. van Duin, S. Dasgupta, F. Lorant, and W. A. Goddard, J. Phys. Chem. A **105**, 9396 (2001).
[28]K. Nomura, R. K. Kalia, A. Nakano, P. Vashishta, A. C. T. van Duin, and W. A. Goddard, Phys. Rev. Lett. **99**, 148303 (2007).
[29]K. Nomura, R. K. Kalia, Y. Li, A. Nakano, P. Rajak, C. Sheng, K. Shimamura, F. Shimojo, and P. Vashishta, Sci. Rep. **6**, 24109 (2016).
[30]J. M. D. Lane, G. S. Grest, A. P. Thompson, K. R. Cochrane, M. Desjarlais, and T. R. Mattsson, AIP Conf. Proc. **1426**, 1435 (2012).
[31]K. Nomura, P. E. Small, R. K. Kalia, A. Nakano, and P. Vashishta, Comput. Phys. Commun. **192**, 91 (2015).
[32]J. M. Gurgel, L. S. A. Filho, and P. P. S. Couto, ECTP Proc. **15**, 1003 (1999).
[33]V. C. Tellez, B. S. Gaytan, S. Bernes, and E. G. Vergara, Acta Crystallogr. Sect. C **58**, 228 (2002).
[34]F. Takusagawa, K. Hirotsu, and A. Shimada, Bull. Chem. Soc. Jpn. **46**, 2020 (1973).